Acta Pharmaceutica Sinica B 2026;16(1):539−554

Chinese Pharmaceutical Association
Institute of Materia Medica, Chinese Academy of Medical Sciences

Acta Pharmaceutica Sinica B

www.elsevier.com/locate/apsb
www.sciencedirect.com

ORIGINAL ARTICLE

pH-Activatable engineered nanoparticle-based selective hexokinase 2 degrader provokes GSDME-dependent pyroptosis for cancer therapy

Linlin Gong[a,b,†], Shasha Li[a,b,†], Jiahui Sun[a,b,†], Kunhong Liu[a,b], Simeng Wang[c], Meiju Ji[c], Peng Hou[c], Li Yan[b], Dan Yang[d], Dechun Liu[a,b,*]

[a]*Research & Development Institute of Northwestern Polytechnical University in Shenzhen, Shenzhen 518057, China*
[b]*Institute of Medical Research, Northwestern Polytechnical University, Xi'an 710072, China*
[c]*Key Laboratory for Tumor Precision Medicine of Shaanxi Province and Department of Endocrinology, The First Affiliated Hospital of Xi'an Jiaotong University, Xi'an 710061, China*
[d]*Department of Pharmaceutical Sciences, School of Biological and Pharmaceutical Sciences, Shaanxi University of Science and Technology, Xi'an 710021, China*

Received 13 February 2025; received in revised form 8 June 2025; accepted 4 August 2025

KEY WORDS

Targeted protein degradation;
Polyethyleneimine;
Nanoparticle;
Nano-PROTACs;
Aerobic glycolysis;
Hexokinase 2;
Pyroptosis;
Cancer therapy

Abstract Proteolysis targeting chimeras (PROTACs) technology has been developed as an exquisite promising approach for targeted protein degradation by hijacking the cellular ubiquitin-proteasome system (UPS). However, traditional PROTACs often suffer from insufficient tumor accumulation, unfavorable membrane penetration, and always-on biological activity, limiting their antitumor performance. Herein, we report a novel pH-activatable engineered nanoparticle-based selective hexokinase 2 degrader (Nano-PROTACs) for cancer therapy. Nano-PROTACs were constructed by conjugating PEI-based PROTACs to amphiphilic nanoparticles *via* acid-detachable *cis*-aconitic anhydride (CAA) bonds. Then, Nano-PROTACs allowed PEI-based PROTACs release within the tumor acidic microenvironment, which bounded to HK-2 and recruited cereblon (CRBN) to provoke HK-2 ubiquitination for achieving HK-2 degradation *via* UPS. Interestingly, Nano-PROTACs specifically evoked GSDME-mediated pyroptosis to enhance cancer therapy. Thus, Nano-PROTACs effectively inhibited the growth of CT26 tumors and

*Corresponding author.
E-mail address: dechun.liu@nwpu.edu.cn (Dechun Liu).
†These authors made equal contributions to this work.
Peer review under the responsibility of Chinese Pharmaceutical Association and Institute of Materia Medica, Chinese Academy of Medical Sciences.

https://doi.org/10.1016/j.apsb.2025.11.002

prevented tumor growth and lung metastasis in the orthotopic 4T1-luciferase tumor-bearing mouse model. Taken together, this study might offer a nanoparticle-based PROTACs platform for advancing selective protein of interest (POI) degradation in cancer therapy.

1. Introduction

Aerobic glycolysis is the unique characteristic of cancers to supply energy for tumor cells no matter whether aerobic or anaerobic condition not, a phenomenon termed "the Warburg effect"[1]. Aerobic glycolysis plays a vital pathophysiological role in cancer progression and metastasis, metabolic disease (*e.g.,* colitis and diabetics)[2,3], and this metabolic reprogramming makes tumor cells meet higher energy requirements[4]. Recently, hexokinase 2 (HK-2) has been identified as the principal rate-limiting enzyme in the process of glycolysis that catalyzes glucose to produce glucose-6-phosphate (G6P)[5]. In addition, HK-2 has been proven to be overexpressed in tumor cells and maintains control of the amount of glucose involved in glycolysis[6,7]. Accumulating evidence supports HK-2 as an attractive and potent target for cancer therapy[8-10].

Previous studies demonstrated that the development of selective HK-2 inhibitors including 2-deoxy-D-glucose (2-DG)[11], 3-bromopyruvic acid (3-BrPA)[12], and lonidamine (LND)[13,14] achieved the initial anti-tumor effect in different cell types. However, the glycolysis inhibition elicited by these small molecules only blocked the activity of proteases *via* occupancy-driven modality and represented biosafety concerns[15]. There is an urgent need to develop a new strategy to intervene in HK-2 expression and inhibit aerobic glycolysis of tumor cells.

Heterobifunctional Proteolysis Targeting Chimeras (PROTACs) endows a promising candidate in the field of cancer therapy as they can degrade pathogenic proteins in a recyclable manner, showing their superiority over traditional small molecule drugs[16-18]. The traditional structure of PROTACs is usually composed of three parts: the protein of interest (POI) binding warhead, the ligand that specifically hijacks endogenous E3 ubiquitin ligase, and a linker connecting with the other two ligands[19-21]. The warhead recognizes and binds the POI, while the other ligand recruits and binds the E3 ubiquitin ligase to trigger ubiquitination of POI for degradation by the ubiquitin-proteasome system (UPS)[22,23]. Intracellular proteins can be potentially degraded by PROTACs, including Bromodomain-Containing Protein 4 (BRD4), Cyclin-Dependent Kinase 6 (CDK6), and Bruton Tyrosine Kinase (BTK)[24-26]. However, traditional PROTACs generally compromise unfavorable membrane penetration, poor pharmacokinetics, insufficient tumor specificity, and always-on biological activity, leading to potential systemic toxicity[27,28]. Therefore, there is a formidable challenge to develop a more efficient POI degradation strategy for biomedical applications.

As a universal gene transfection tool, polyethyleneimine (PEI) polymers possess high capabilities of rupture of membranes, and easy formulation owing to abundant amino groups[29,30]. Despite being promising, conventional PEI polymers suffer from rapid clearance from blood circulation and potential toxicity toward normal cells due to superior positive charge. In addition, because a series of biological barriers impede nanoparticles from penetrating into tumor tissues[31-34], a series of intelligent nanomedicine delivery systems have been reported that relatively initial large size of nanomedicine achieves longer half-time in blood circulation and tumor accumulation while transformation into small nanoparticles or charge reversal responding to tumor microenvironment confers to facilitate tumor penetration[35-40]. Thus, we hypothesized that smart pH-activatable engineered nanoparticle-based selective HK-2 degrader could be designed based on tumor microenvironment and a novel and universal POI degradation platform could be developed.

Herein, we engineered a novel pH-activatable engineered nanoparticle-based selective protein degrader (Nano-PROTACs) platform. For proof-of-concept, HK-2 and E3 ubiquitin ligase targeting probes were first conjugated to PEI polymers with optimized ratio. Then, in order to achieve activatable protein degradation ability, PEI-based PROTACs was conjugated to U.S. Food and Drug Administration (FDA) approved poly(ethylene glycol)-poly (*ε*-caprolactone) (PEG-PCL) diblock copolymers *via* acid-detachable *cis*-aconitic anhydride (CAA) bonds. As a negative control, pH-stable Nano-PROTACs (sNano-PROTACs) were synthesized by conjugating PEI-based PROTACs to PEG-PCL *via* acid-stable succinic anhydride bonds. Nano-PROTACs allowed PEI-based PROTACs specific accumulation in the tumor tissues *via* enhanced permeability and retention (EPR) effect and enhanced tumor penetration in response to tumor acidic microenvironment. Compared to traditional PROTACs, the present Nano-PROTACs platform exhibited following important advantages: (1) flexible ligand ratios regulation; (2) precisely pH-activatable protein degradation ability; (3) Nano-PROTACs improved the delivery efficiency with the characteristics of transformable size and charge reversal; (4) increased ubiquitination ability *via* orchestrally inducing HK-2 polyubiquitination *via* hijacking ubiquitin-proteasome system (UPS). Importantly, we also found that Nano-PROTACs could specifically elicit GSDME-mediated pyroptosis to enhance cancer therapy. Taken together, Nano-PROTACs efficiently degraded HK-2 in CT26 and 4T1 tumor cells *in vitro* and *in vivo*, activating GSDME-mediated pyroptosis for augmented cancer therapy. This study might provide a novel and general nanoplatform to achieve POI degradation (Fig. 1).

2. Materials and methods

2.1. Reagents

Lonidamine (LND), 2-(2,6-dioxo-piperidin-3-yl)-4-fluoroisoindoline-1,3-dione, 2-(7-aza-1*H*-benzotriazole-1-yl)-1,1,3,3-tetramethyluronium hexafluorophosphate (HATU), 4-dimethylaminopyridine (DMAP), *N*,*N*-diisopropylethylamine (DIPEA) and 3-(4,5-dimethylthiazol-2-yl)-2,5-diphenyltetrazolium bromide (MTT) were purchased from Sigma−Aldrich. Methoxy poly(ethylene glycol) (Mn = 5000 g/mol, $mPEG_{5000}$-OH) and 6-hexanolactone (*ε*-CL) were purchased from Adamas Beta. Annexin V-FITC/PI Apoptosis Detection Kit and JC-1

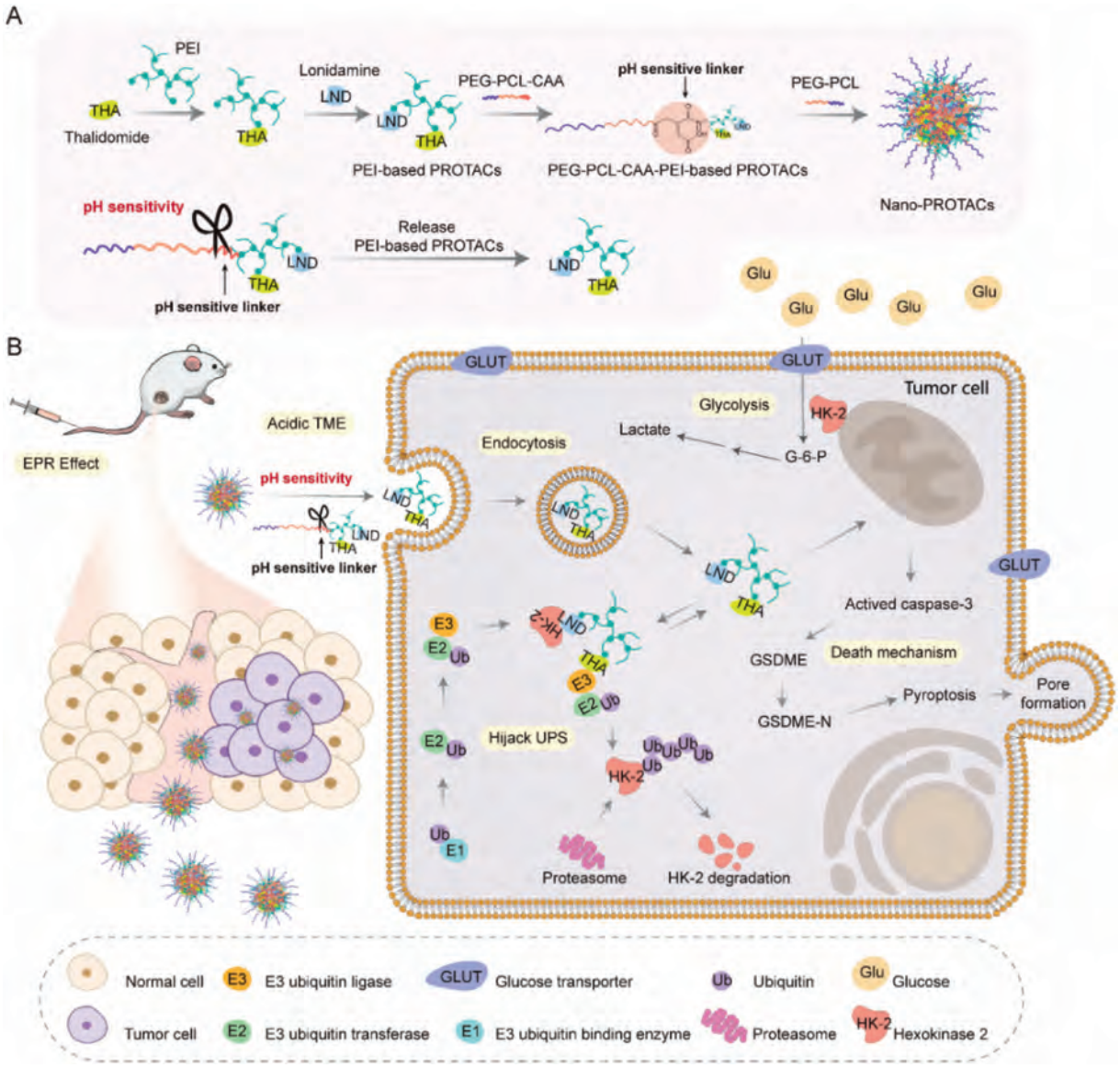

Figure 1 Schematic illustration of Nano-PROTACs mediated HK-2 degradation for inhibiting tumor aerobic glycolysis and inducing tumor cells pyroptosis. (A) Chemical structures and preparation of PEI-based PROTACs and Nano-PROTACs, including E3 ubiquitin ligase binding unit (THA), HK-2 binding unit (LND) and PEI (function as the linker of PROTACs). (B) Nano-PROTACs accumulated in tumor cells by EPR effect. Then it entered tumor cells by endocytosis. After Nano-PROTACs sensed acid environment (pH $\leq$ 6.5), the acid sensitive bond was broken and PEI-based PROTACs was released. PEI-based PROTACs bound to HK-2 and E3 ubiquitin ligase. It had two functions. First, PEI-based PROTACs hijacked the UPS and degraded HK-2 at the surface of mitochondria. As a result, tumor aerobic glycolysis was suppressed and tumor micro-environment was reshaped. Second, PEI-based PROTACs induced active caspase-3 which cut GSDME, and then facilized cell pyroptosis. Finally, all of above processes enhanced tumor inhibition effect.

mitochondria membrane potential detection kit were obtained from Beyotime, Shanghai, China. Rabbit anti-HK-2 antibody, rabbit anti-GSDME antibody, mouse anti-β-actin antibody, rabbit anti-Caspase 3 antibody, and mouse anti-GSDMD antibody were obtained from Proteintech.

2.2. *Synthesis of PEI-based PROTACs*

PEI-based PROTACs was synthesized as following method. Polyethyleneimine (PEI, 20 mg) and thalidomide (THA, 3.07 mg) were dissolved in DMF (2.5 mL) and mixed in the eggplant-shaped flask. After vacuuming the flask, DIPEA (1.94 μL) was dropped. The mixture was stirred for 12 h at 90 °C. Cooling the reaction at room temperature. Then, lonidamine (LND, 3.57 mg) and HATU (8.45 mg) were respectively dissolved in DMF and dropped in the flask. The mixture was further stirred for 4 h at 37 °C. The product was dissolved in dichloromethane (DCM) and purified by cold ethyl ether. After centrifuging (15,000 rpm, 10 min) (Eppendorf, 5430R, Germany), the purified product was obtained.

2.3. Synthesis of poly(ethylene glycol)$_{5k}$-poly(ε-caprolactone)$_{5k}$ (PEG$_{5k}$-PCL$_{5k}$)

The polymer PEG$_{5k}$-PCL$_{5k}$ was synthesized by a ring-opening reaction as follows. mPEG$_{5k}$ (1 g) was added in a pre-vacuum flask and heated at 80 °C for 1 h. ε-Caprolactone (1 g) was added to the flask and vacuumed for 0.5 h. Then, a drop of stannous octoate was added to the flask and the mixture was stirred at 120 °C for 6 h. After cooling, the product was dissolved in DCM and purified by cold ethyl ether. After centrifuging (15,000 rpm, 10 min), the purified product was obtained. After drying overnight, the product was stored at −30 °C.

2.4. Synthesis of PEG$_{5k}$-PCL$_{5k}$-CAA-PEI-based PROTACs

PEG$_{5k}$-PCL$_{5k}$-CAA-PEI-based PROTACs were synthesized as follows. *cis*-Aconitic anhydride (CAA, 12.4 mg) was dissolved in DCM. The solution was added to a pre-vacuum flask and stirred in an ice bath. Oxalyl chloride (11 μL) and *N*,*N*-dimethylformamide (DMF, 1 drop) were dropped in the above solution. The mixture was stirred for 10 min in an ice bath and 1 h at room temperature. The solvent and unreacted reactants were removed by rotary evaporator (EYELA, CCA-1112A, Shanghai). Then the product was redissolved in DCM. PEG$_{5k}$-PCL$_{5k}$ (400 mg) and triethylamine (Et_3N, 12 μL) were dissolved in DCM and dropped in the flask. The mixture was stirred in an ice bath for 10 min and at room temperature for another 2 h. The PEI-based PROTACs was then added to the above solution and stirred for 12 h. The final product was added to a dialysis bag (7000 Da) and immersed in 50% alcohol solution for 24 h. Then the outer fluid was replaced with water for 4 h. The purified solid product was obtained by lyophilization. ^{1}H NMR (500 MHz, Chloroform-$_d$) δ 3.23 (s, 3H, a), 3.50 (s, 450H, b), 3.98 (t, 68H, c), 1.53 (dq, 136H, d), 1.29 (h, 6.4 Hz, 68H, e), 2.27 (t, 68H, f), 5.87−5.70 (m, 1H, g).

2.5. Synthesis of PEG$_{5k}$-PCL$_{5k}$-SA-PEI-based PROTACs

PEG$_{5k}$-PCL$_{5k}$-SA-PEI-based PROTACs was prepared as the following method. PEG$_{5k}$-PCL$_{5k}$ (400 mg), succinic anhydride (SA, 12 mg), and DMAP (9.8 mg) were dissolved in tetrahydrofuran (THF). PEG$_{5k}$-PCL$_{5k}$ solution and SA solution were mixed in the flask and vacuumed for 30 min. After dropping DMAP, the mixture was stirred at 37 °C for 12 h. The final solid product was obtained through an amide reaction and purified following the same method of PEG$_{5k}$-PCL$_{5k}$-CAA-PEI-based PROTACs. ^{1}H NMR (500 MHz, Chloroform-d) δ 4.05 (t, 40H), 3.63 (m, 450H), 3.37 (s, 3H), 2.53 (m, 4H), 2.30 (t, 40H), 1.63 (m, 80H), 1.37 (m, 40H).

2.6. Synthesis of PEG$_{5k}$-PCL$_{5k}$-CAA-PEI-based PROTACs-Ce6 and PEG$_{5k}$-PCL$_{5k}$-SA-PEI-based PROTACs-Ce6

PEG$_{5k}$-PCL$_{5k}$-CAA-PEI-based PROTACs-Ce6 was prepared as follows. PEG$_{5k}$-PCL$_{5k}$-CAA-PEI-based PROTACs (10 mg), Ce6 (0.47 mg), HATU (0.6 mg) and DIPEA (0.7 μL) were dissolved in DMF. PEG$_{5k}$-PCL$_{5k}$-CAA-PEI-based PROTACs and Ce6 were mixed together and vacuumed for 10 min. HATU and DIPEA were dropped in the above solution. The mixture was stirred at room temperature overnight. The final product was added to a dialysis bag (7000 Da) and immersed in DMF for 24 h. Then the outer fluid was replaced with water for 4 h. The solid purified product was obtained by lyophilization. PEG$_{5k}$-PCL$_{5k}$-SA-PEI-based PROTACs-Ce6 synthesis method was the same as above by replacing PEG$_{5k}$-PCL$_{5k}$-CAA-PEI-based PROTACs with PEG$_{5k}$-PCL$_{5k}$-SA-PEI-based PROTACs.

2.7. Preparation of Nano-PROTACs, sNano-PROTACs, Ce6 labeled-nano-PROTACs and Ce6 labeled-sNano-PROTACs

Nano-PROTACs was prepared by the following method. PEG$_{5k}$-PCL$_{5k}$-CAA-PEI-based PROTACs (3.9 mg) and PEG$_{5k}$-PCL$_{5k}$ (3.9 mg) was respectively dissolved in DMF (100 μL) and mixed. Then, the mixture was dropped into ultrapure water in a stirring state for 15 min. The final nanoparticle solution was added in a dialysis bag (14,000 Da) and immersed in 500 mL ultrapure water for 12 h to remove the DMF solution. Finally, Nano-PROTACs was obtained. sNano-PROTACs, Ce6 labeled-Nano-PROTACs and Ce6 labeled-sNano-PROTACs were prepared by the same method like above except replacing PEG$_{5k}$-PCL$_{5k}$-CAA-PEI-based PROTACs with PEG$_{5k}$-PCL$_{5k}$-SA-PEI-based PROTACs, PEG$_{5k}$-PCL$_{5k}$-CAA-PEI-based PROTACs-Ce6 with PEG$_{5k}$-PCL$_{5k}$-SA-PEI-based PROTACs-Ce6.

2.8. Characteristics

Particle size and zeta potential of Nano-PROTACs and sNano-PROTACs were evaluated by Dynamic Light Scattering Particle Size Analyzer (NanoBrook 90plus PALS). The morphology of Nano-PROTACs and sNano-PROTACs were characterized by TEM (JEM-1200EX, JEOL) using 2% uranyl acetate as a negative staining agent. The characteristic absorption peak of PEI-based PROTACs was measured by an ultraviolet spectrophotometer (Hitachi U-3900). PEG$_{5k}$-PCL$_{5k}$, PEG$_{5k}$-PCL$_{5k}$-CAA-PEI-THA-LND, PEG$_{5k}$-PCL$_{5k}$-SA-PEI-THA-LND structures were detected by ^{1}H NMR, using $CDCl_3$ as the solvents.

2.9. Cell line and cell culture

CT26 cell line was obtained from the Institute of Basic Medical Science, Chinese Academy of Medical Science. CT26 cells were cultured in RPMI 1640 medium which contained 10% (*v*/*v*) FBS, 100 IU/mL penicillin, and 0.1 mg/mL streptomycin at 37 °C with 5% CO_2. CT26 cells were grown in the logarithmic stage.

2.10. Western blot assay

CT26 cells were cultured in 6 well cell culture plates. After different treatments of drugs, all groups of cells were collected in 1.5 mL centrifuge tubes and centrifuged for 10 min at 3000 rpm (Eppendorf). Then cells were washed and centrifuged again. The liquid supernatant was discarded and RIPA (containing 1 mmol/L PMSF) was mixed with cells for 30 min. The mixture was treated with the ultrasonic machine for 4 min in an ice bath and centrifuged for 10 min at 15,000 rpm (Eppendorf). After boiling for 10 min at 95 °C, the samples were obtained. Electrophoresis was used for analyzing the sample. After proteins were transferred to polyvinylidene difluoride (PVDF) membranes at 250 mA, 5% skim milk was used for blocking the membrane. Then membranes were put in the first antibody for 12 h and the second antibody for 2 h. The results were detected by a Chemiluminescence imaging system (VILBER, FUSION FX EDGE/DBT, Beijing, China).

2.11. PEI-based PROTACs release from Nano-PROTACs

200 μL Nano-PROTACs and sNano-PROTACs were respectively added in dialysis bags (14,000 Da) and respectively immersed in 4 mL PB solutions (pH 6.5, pH 7.4). The outer fluid of the dialysis bag was collected at different times. The content of PEI-based PROTACs in outer fluid at different times was detected by ultraviolet at 278 nm.

2.12. PEI-based PROTACs, Nano-PROTACs, and sNano-PROTACs glycolysis detection

Seahorse (ECAR) was used for glycolysis detection. Before the detecting day, CT26 cells were seeded in 96 well plates for 24 h. Nano-PROTACs (LND: 10 μg/mL) and sNano-PROTACs (LND: 10 μg/mL) were added to the cell plate and cultured for 24 h. Cartridges were immersed in sterile water for 12 h. On detection day, cartridges were hydrated in calibrant and incubated in a non-CO_2 incubator at 37 °C. Detection fluid was used for washing cells two times. Then cell plate was incubated in a non-CO_2 incubator at 37 °C. Glucose, oligomycin, and 2-DG were added in drug-adding cores which made the end concentration reach glucose (10 mmol/L), oligomycin (1 μmol/L), and 2-DG (50 mmol/L). Finally, the plate was detected by Agilent Seahorse XFe96 Analyzer.

2.13. Nano-PROTACs and sNano-PROTACs stability assay

The stability of Nano-PROTACs and sNano-PROTACs were detected by nanoparticle size and PDI change. Ultrapure water and PBS (pH 7.4) were used to dilute Nano-PROTACs and sNano-PROTACs. The particle size and PDI of Nano-PROTACs and sNano-PROTACs were detected for 7 days.

2.14. Nano-PROTACs dissociation detection

Nano-PROTACs dissociation ability in acid environment was detected by nanoparticle size and zeta potential change in PBS (pH 6.5). Nano-PROTACs and sNano-PROTACs were incubated with pH 6.5 PBS and pH 7.4 PBS at different times at 37 °C. Particle size and zeta potential were detected by Dynamic Light Scattering. The former was detected at 0, 4, and 24 h and the latter was detected at 0, 3, and 6 h.

2.15. Nano-PROTACs and mitochondria colocalization

CT26 cells were cultured in confocal cell culture dishes for 24 h Ce6-labeled Nano-PROTACs were added in cells for 3 h. Then, washing cells three times and Mito-tracker solution was added to it for 20 min at 37 °C. After incubation, PBS was used for washing cells and Hoechst 33,342 were added and cultured with cells for 15 min. Confocal microscopy was used to detect the result.

2.16. The penetration ability of Nano-PROTAC and sNano-PROTAC in the tumor sphere

Before drug penetration detection, CT26 tumor spheres were constructed in 96 well plates. Agarose (10 mg/mL) was added to 96 well plate. CT26 cells (3000 cells/well) were seeded in an agarose 96 well plates for 5 days. Then, Ce6-labeled Nano-PROTACs and Ce6-labeled sNano-PROTACs were incubated with tumor spheres for 24 h in pH 6.5 and pH 7.4 cell culture medium. After washing tumor spheres three times, confocal microscopy was used to detect the penetration result.

2.17. Cytotoxicity evaluation of LND, PEI-based PROTACs, Nano-PROTACs and sNano-PROTACs

CT26 cell viability under LND, PEI-based PROTACs, Nano-PROTACs, and sNano-PROTACs treatment were detected by MTT and Calcein-AM/PI staining. For MTT detection, cells were seeded in 96 well plates for 24 h. Different concentration drugs were added to the plate and incubated for another 24 h. Then MTT (500 μg/mL) was used to culture cells for 3 h at 37 °C. After getting rid of the supernatant liquid, DMSO was added to the plate. The Microplate multimode microplate reader (Tecan, Spark, Switzerland) was used to detect the result at 490 nm. For Calcein-AM/PI staining detection, CT26 cells were cultured in cell crawling slides for 24 h. LND, PEI-based PROTACs, Nano-PROTACs, and sNano-PROTACs were added and incubated with cells for another 24 h. Calcein-AM and PI were used to stain cells. Then cells were washed twice time and 4% PFA was used to fix the cells. The result was detected by Confocal microscopy (OLYMPUS, FV3000, Japan).

2.18. Cell apoptosis assay

Annexin V-FITC cell apoptosis kit was used to detect cell apoptosis. CT26 cells were cultured in 6 well plates for 24 h. LND, PEI-based PROTACs, Nano-PROTACs, and sNano-PROTACs were added to the plate for 24 h. Pancreatic enzymes without EDTA were used to digest the cells. Collect cells in 1.5 mL centrifuge tubes and centrifuge them at 300 g for 5 min. Annexin V-FITC was added to cells and incubated for 15 min at 37 °C. After incubation, 350 μL binding buffer and 10 μL PI were added to each tube. The result was detected by flow cytometry (BD Biosciences, FACSCelesta™, USA).

2.19. Mitochondria potential assay

Mitochondria potential was detected by JC-1. CT26 cells were cultured in cell-crawling slides for 24 h. LND, PEI-based PROTACs, Nano-PROTACs, and sNano-PROTACs were added and incubated for another 24 h. 4% PFA was used to fix cells. JC-1 dye was added and incubated with cells for 20 min. After incubating, cells were washed with a pre-cooling buffer two times. Confocal microscopy (OLYMPUS) was used to detect the result.

2.20. In vivo therapeutic effect

BALB/c mice were grown in a constant temperature and humidity environment with enough water and food. All animal procedures were approved by the Medical and Experimental Animal Ethics Committee at Northwestern Polytechnical University (Approval No. 202001055). Mice were divided into 4 groups ($n = 5$). CT26 cells were injected into the right back of mice. After tumor size arrived at 50 mm^3, PEI-based PROTACs, Nano-PROTACs, and sNano-PROTACs were administrated *via* intravenous injection (i.

v.) in mice for 6 times intervals one day. Tumor volume and mice body weight were recorded every two days. When the mean tumor size arrived at 1500 mm^3, the *in vivo* therapeutic experiment was stopped. Heart, liver, spleen, lung, kidneys, and tumors of mice in every group were harvested and analyzed by H&E stains and Western blot.

To further investigate Nano-PROTACs anti-tumor effect, a 4T1-luc orthotopic tumor model was constructed. When tumor volume was 50 mm^3, the mice were divided into 4 groups: PBS, PEI-based PROTACs, sNano-PROTACs, and Nano-PROTACs were injected *via* intravenous injection. Tumor volume was recorded. When the tumor volume was 1500 mm^3, the mice were regarded as dead. Tumors and other major organs from mice were examined by immunofluorescent staining and H&E staining.

2.21. *Immunofluorescence staining*

Tumors were sliced by frozen microtome. Tumor sections were fixed by 4% PFA for 15 min. Triton was used for permeable cell membranes and 5% BSA was used for blocking tumor sections. After 1 h blocking, tumor biopsies were incubated with the first antibody for 12 h at 4 °C. PBS was used for washing them. The second antibody was incubated with tumor biopsies for another 2 h. Confocal microscopy (OLYMPUS) was used to detect the result.

2.22. *Tumor pulmonary metastatic study in vivo*

4T1-luc orthotopic tumor model was constructed. The mice were divided into 4 groups and injected *via* intravenous injection with

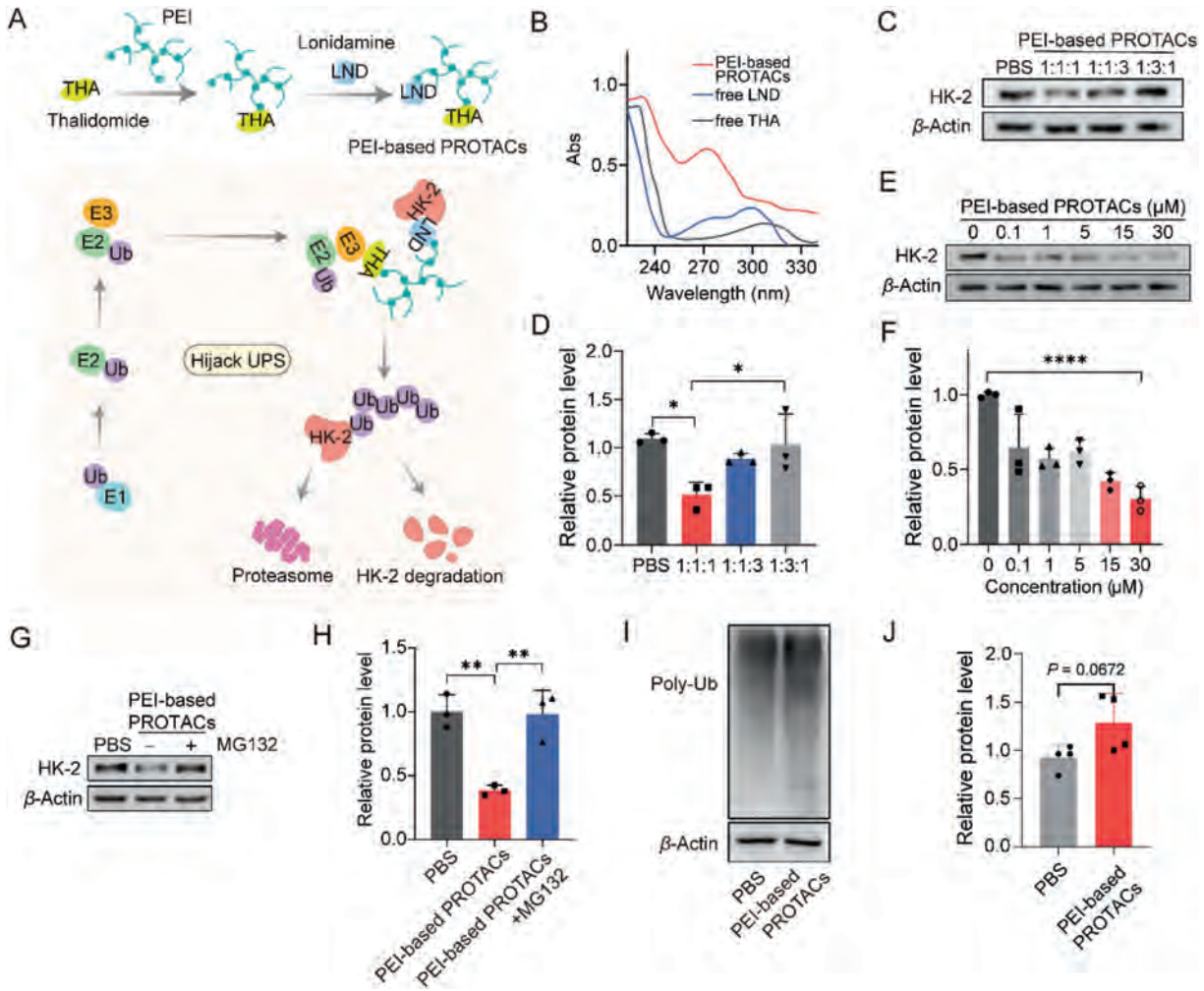

Figure 2 Degradation of HK-2 by PEI-based PROTACs. (A) The scheme of PEI-based PROTACs synthesis and HK-2 degradation mechanism. (B) The UV absorption of free LND, free THA and PEI-based PROTACs. (C) Western blot assay of PEI-based PROTACs degradation effect with different LND and THA ratio. The ratios referred to the mass ration of PEI polymers: LND: THA. (D) The quantitation result of C. (E) The degradation effect of PEI-based PROTACs was dependent on concentration in CT26 cells. CT26 cells were treated with different concentration PEI-based PROTACs for 6 h. (F) The quantitative result of PEI-based PROTACs degradation effect dependent on concentration. (G) The HK-2 degradation mechanism of PEI-based PROTACs. CT26 cells were pre-treated with MG132 (100 nmol/L) for 1 h, and then treated with PEI-based PROTACs upon co-incubation with the same concentration of MG132 for 24 h. (H) The quantitation of PEI-based PROTACs HK-2 degradation mechanism. (I) Western blot assay and (J) quantitation of CT26 cells poly-ubiquitin effect after treating with PEI-based PROTACs. $^*P < 0.5$, $^{**}P < 0.01$, $^{****}P < 0.0001$.

PBS, PEI-based PROTACs, sNano-PROTACs, and Nano-PROTACs for five cycles at intervals of 1 day. After 25 days, 200 μL D-Luciferin (15 mg/mL) was injected in mice *via* intraperitoneal injection. After 6 min, the bioluminescence signal was detected by the In Vivo Imaging System (PerkinElmer, IVIS Lumina LT Series III, USA). Then the pulmonary of mice was obtained. D-Luciferin solution was used to immerse the mice pulmonary for 8 min. The results were detected by In Vivo Imaging System (PerkinElmer).

2.23. Statistical analysis

Most of the experiment data are expressed as means ± standard deviation (SD). All of the significant differences were calculated by *t*-tests and One-way ANOVA. GraphPad Prism was used to perform the statistical analysis. $^{*}P < 0.5$, $^{**}P < 0.01$, $^{***}P < 0.001$, $^{****}P < 0.0001$.

3. Results and discussion

3.1. Preparation and characterization of PEI-based PROTACs

Lonidamine (LND), an antagonist of the rate-limiting enzyme (HK-2) of tumor aerobic glycolysis, is used as a tumor energy intervention device for cancer therapy. However, LND is often used in combination with other chemotherapy agents to treat tumors owing to poor anti-tumor efficacy[41]. Here, a novel polyethyleneimine (PEI)-based PROTACs was developed, consisting

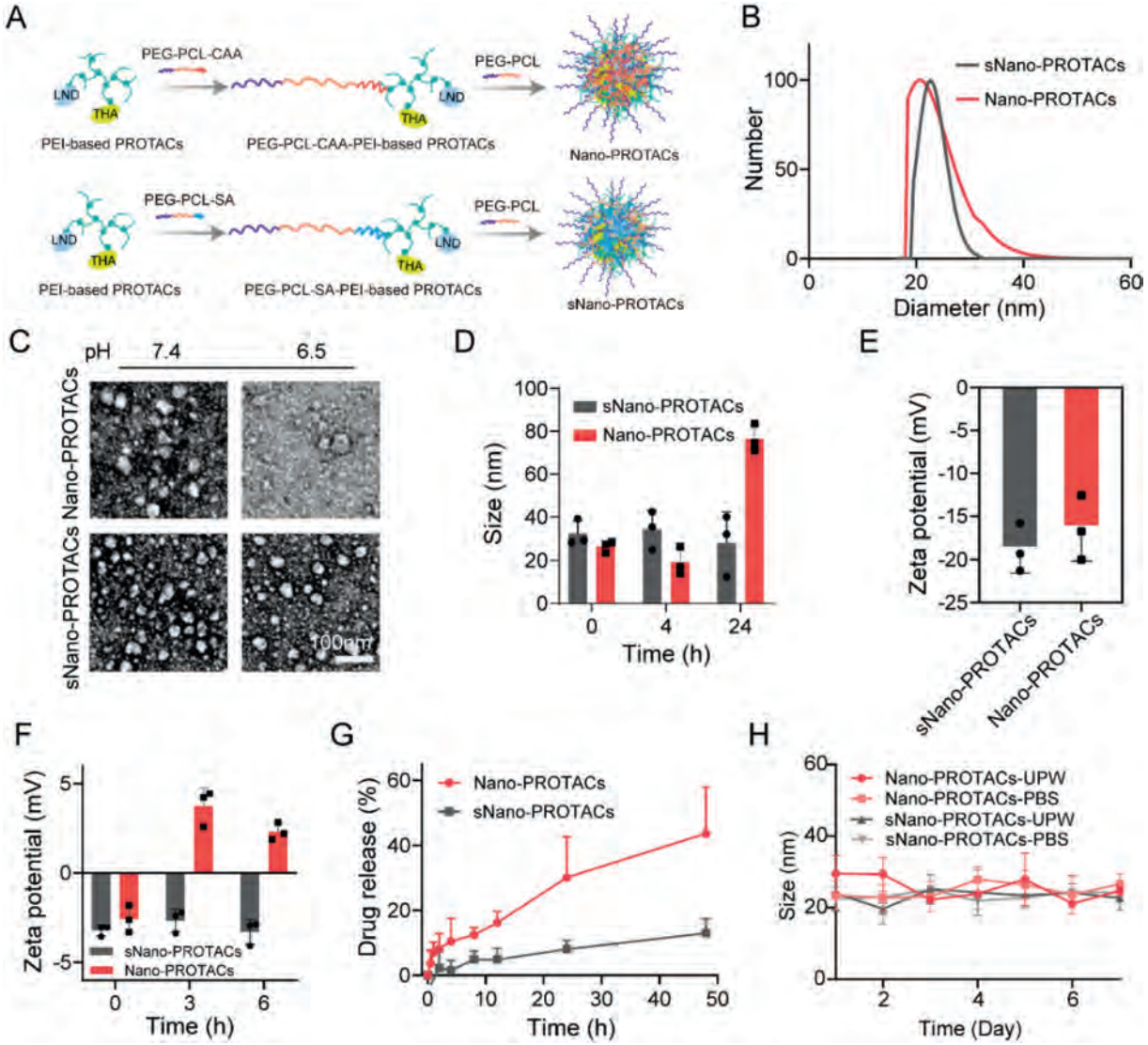

Figure 3 Preparation and acid-responsive properties of engineered nano-PROTACs. (A) The illustration of Nano-PROTACs and sNano-PROTACs preparation. (B) Particle size of Nano-PROTACs and sNano-PROTACs in ultrapure water, which was detected by DLS. (C) TEM of Nano-PROTACs and sNano-PROTACs in pH 7.4 PBS and pH 6.5 PBS. Scale bar = 100 nm. (D) Nano-PROTACs and sNano-PROTACs particle size change in pH 7.4 PBS and pH 6.5 PBS after incubation for 0, 4, and 24 h at 37 °C, detected by DLS. (E) Zeta potential of Nano-PROTACs and sNano-PROTACs in ultrapure water. (F) Nano-PROTACs and sNano-PROTACs zeta potential change in pH 7.4 PBS and pH 6.5 PBS after incubation for 0, 3, and 6 h at 37 °C. (G) PEI-based PROTACs release detection from Nano-PROTACs and sNano-PROTACs in pH 6.5 PBS at 37 °C. (H) Nano-PROTACs and sNano-PROTACs particle stability detection in pH 7.4 PBS and ultrapure water for 7 days. Nano-PROTACs and sNano-PROTACs were stored at 4 °C.

of a HK-2 binding module (LND), a CRBN ubiquitin binding module (thalidomide, THA), and a PEI linker module. It was worth noting that cationic polymer PEI acted as PROTACs linker to connect the HK-2 binding module with the CRBN ubiquitin binding module. PEI-based PROTACs were synthesized by conjugating HK-2 targeting unit (LND) and CRBN ubiquitin targeting unit (THA) with amino groups of cationic polymer PEI (Fig. 2A), followed by purification *via* dialysis in ethanol solution. PEI-based PROTACs exhibited ultraviolet-visible absorption with two characteristic peaks at 278 nm (LND) and 237 nm (THA) and infrared spectrum with the specific peak of acylamino, respectively, indicating that LND and THA were successfully conjugated with PEI polymers (Fig. 2B and Supporting Information Fig. S1). We first investigated the effect of the mass ratio of targeting

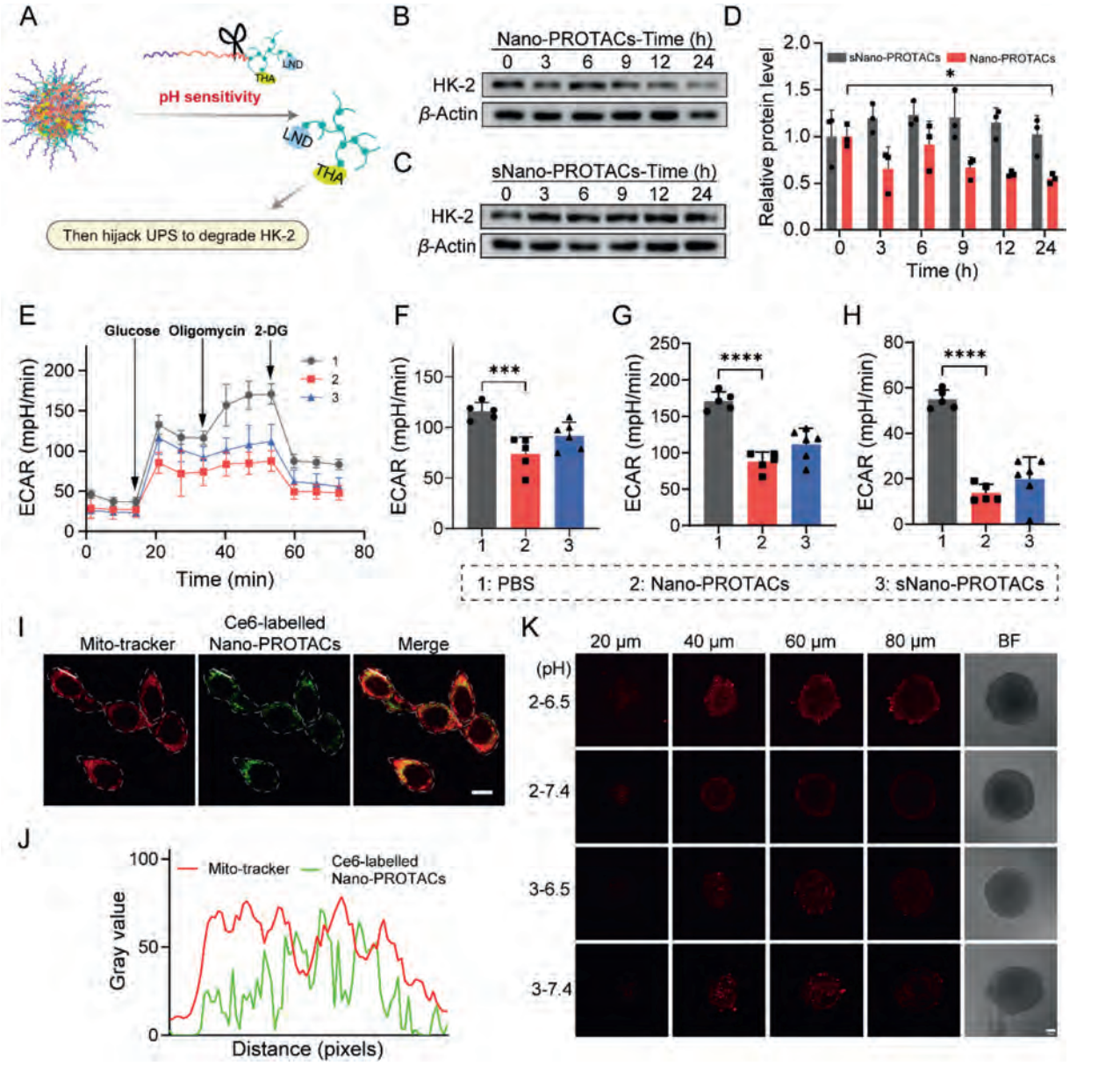

Figure 4 pH-Activatable nano-PROTACs induced HK-2 degradation and reprogrammed glycolysis. (A) The scheme of Nano-PROTACs release PEI-based PROTACs and degrade HK-2 mechanism. (B) The time dependence of HK-2 degradation induced by Nano-PROTACs. (C) The time dependence of HK-2 degradation induced by sNano-PROTACs. (D) The quantitation result of Nano-PROTACs and sNano-PROTACs HK-2 degradation effect dependent time. (E) ECAR of CT26 cells after treated with PEI-based PROTACs, Nano-PROTACs and sNano-PROTACs for 12 h. (F) Glycolysis quantitation of CT26 cells after incubation with PEI-based PROTACs, Nano-PROTACs and sNano-PROTACs. (G) Glycolysis capacity quantitation of CT26 cells after incubation with PEI-based PROTACs, Nano-PROTACs and sNano-PROTACs. (H) Glycolysis reserve quantitation of CT26 cells after incubation with PEI-based PROTACs, Nano-PROTACs and sNano-PROTACs. (I) Colocalization between Ce6-labeled Nano-PROTACs and Mito-tracker. CT26 cells were pre-treated with Ce6-labeled Nano-PROTACs for 3 h, scale bar = 10 μm. (J) The colocalization quantitation between Ce6-labeled Nano-PROTACs and Mito-tracker. (K) Tumor sphere permeation of Nano-PROTACs and sNano-PROTACs in pH 6.5 and pH 7.4 environment. CT26 tumor spheres were incubated with Ce6-labeled Nano-PROTACs and Ce6-labeled sNano-PROTACs for 24 h, scale bar = 50 μm $^{*}P < 0.5$, $^{***}P < 0.001$, $^{****}P < 0.0001$.

probes and cationic polymer PEI on degradation efficiency. As shown in Supporting Information Fig. S2A−S2F, the mass ratio of targeting probes and cationic polymer PEI at 1:1 endowed better degradation efficiency (43.9%) than other proportions after incubating with CT26 cells for 24 h. Next, the ratio of HK-2 and CRBN targeting module was optimized to achieve effective HK-2 degradation. The HK-2: CRBN targeting module at a mass ratio of 1:1 showed better degradation efficiency than other ratios, achieving 46.8% HK-2 degradation (Fig. 2C and D). The degradation of HK-2 by PEI-based PROTACs was dependent on

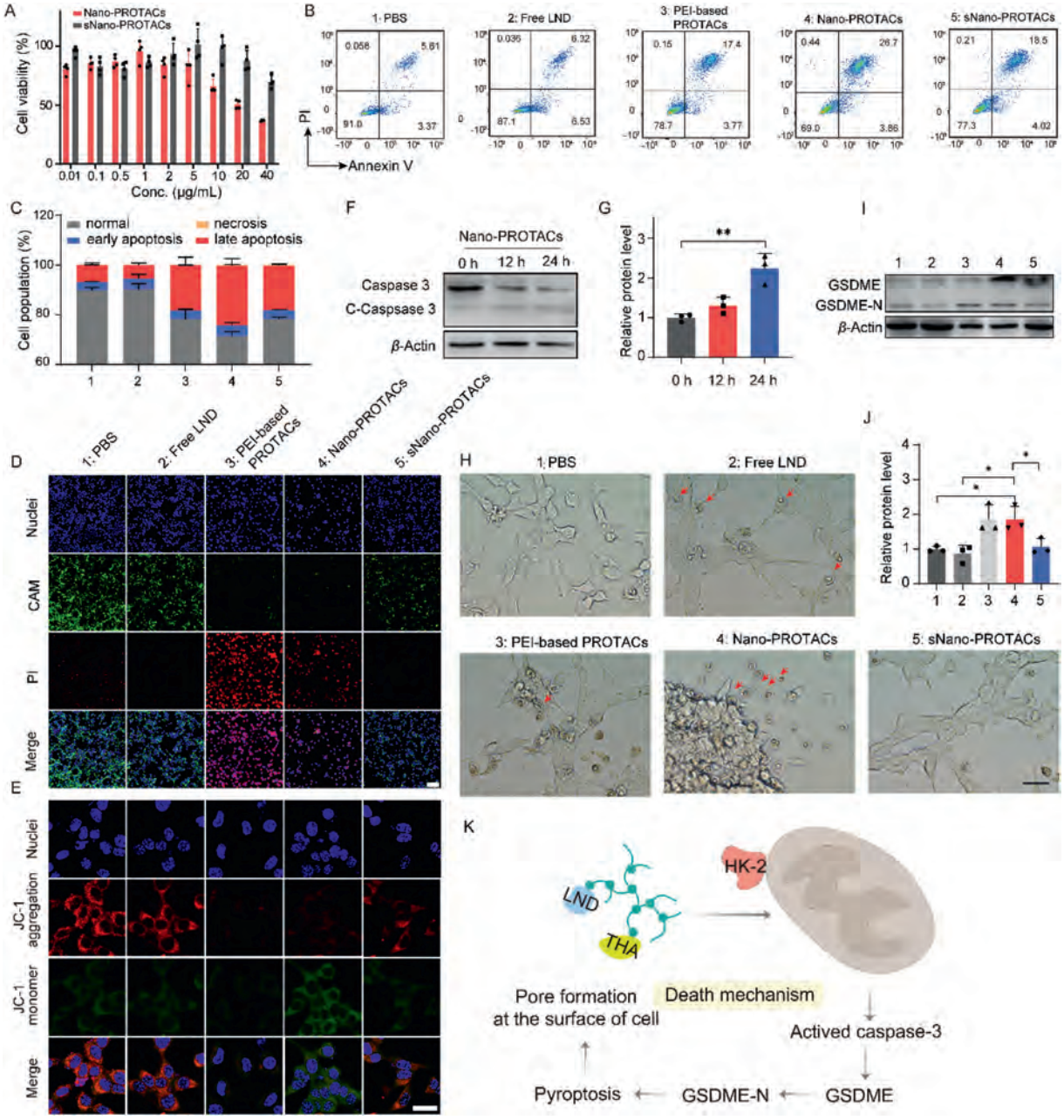

Figure 5 Nano-PROTACs achieved perfect anti-tumor efficiency *via* pyroptotic pathway. (A) CT26 cells viability detection after treated with Nano-PROTACs and sNano-PROTACs with different concentrations for 24 h. (B) CT26 cells apoptosis evaluation after incubated with free LND, PEI-based PROTACs, Nano-PROTACs and sNano-PROTACs for 24 h using Annexin V/PI assay. (C) The quantitation result of CT26 cells apoptosis. (D) CAM/PI staining of CT26 cells after treated with free LND, PEI-based PROTACs, Nano-PROTACs and sNano-PROTACs for 24 h. Red: PI, Green: CAM, scale bar = 100 μm. (E) JC-1 staining result of CT26 cells after treated with free LND, PEI-based PROTACs, Nano-PROTACs and sNano-PROTACs for 24 h. Red: JC-1 aggregation, Green: JC-1 monomer, scale bar = 10 μm. (F) Western blot assay of active caspase 3 induced by Nano-PROTACs. (G) The quantitation result of active caspase 3. (H) Images of CT26 cells after treated with free LND, PEI-based PROTACs, Nano-PROTACs and sNano-PROTACs for 24 h. Scale bar = 50 μm. (I) Western blot assay of GSDME-N induced by free LND, PEI-based PROTACs, Nano-PROTACs and sNano-PROTACs. (J) The quantitation result of active GSDME-N. (K) The scheme of Nano-PROTACs inducing CT26 cells death mechanism. $*P < 0.5$, $**P < 0.01$, $***P < 0.001$, $****P < 0.0001$.

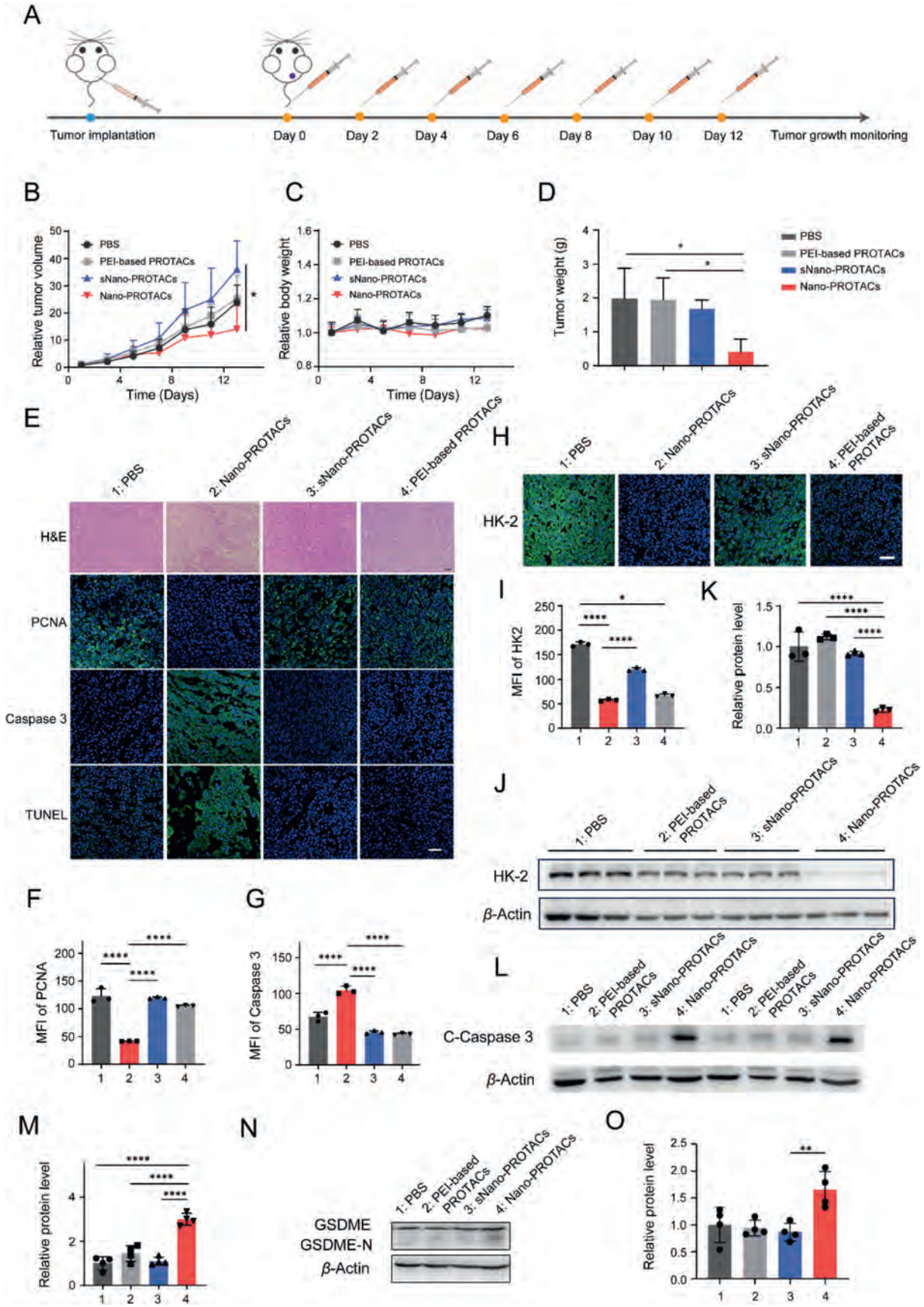

Figure 6 *In vivo* antitumor capacity of Nano-PROTACs. (A) Treatment schedule of PEI-based PROTACs, Nano-PROTACs and sNano-PROTACs antitumor and biosafety study in CT26 tumor bearing mice. CT26 tumor model was established by subcutaneous injection of

concentration according to the Western blot test (Fig. 2E). PEI-based PROTACs exhibited potent degradation of HK-2 in CT26 cells, which was shown in Fig. 2F. Furthermore, the proteasome inhibitor MG132 effectively inhibited the degradation of HK-2 in CT26 cells induced by PEI-based PROTACs, with HK-2 degradation content increased to 97.9%, indicating that PEI-based PROTACs degraded HK-2 in a ubiquitin-proteasome system (UPS) dependent category (Fig. 2G and H). The degradation of HK-2 induced by PEI-based PROTACs and the related degradation mechanisms were also verified in 4T1 cells, which were consistent with the results in CT26 cells (Supporting Information Fig. S3). PEI-based PROTACs degradation process involved ubiquitin participation, so we detected CT26 cell poly-ubiquitin after PEI-based PROTACs treatment. The result was shown in Fig. 2I and J, CT26 cells performed more poly-ubiquitin than the PBS group to a certain extent, whereas there was no significant difference. We further evaluated the cytotoxicity of PEI-based PROTACs toward CT26 and 4T1 tumor cells using MTT assay. As seen in Supporting Information Fig. S4 and Table S1, PEI-based PROTACs had a half inhibition concentration (IC_{50}) of 40.8 and 55.4 μmol/L in CT26 and 4T1 cells, which was 2.8- and 1.3-fold lower than the IC_{50} of free LND, respectively. These data demonstrated that PEI-based PROTACs could effectively induce HK-2 degradation in a UPS-dependent pattern and provoke potent proliferation inhibition toward CT26 and 4T1 tumor cells.

3.2. Preparation and characterization of pH-activatable engineered nanoparticle-based selective hexokinase 2 degrader

To endow on-demand protein degradation ability, we further designed pH-activatable engineered nanoparticle-based selective hexokinase 2 nano-degrader by covalently grafting PEI-based PROTACs onto the backbone of an amphiphilic diblock polymer *via* acid-cleavable bonds. We chose the FDA-approved poly (ethylene glycol)-poly(ε-caprolactone) copolymers (PEG-PCL) as amphiphilic polymers. pH-Activatable Nano-PROTACs (Nano-PROTACs) were synthesized by conjugating PEI-based PROTACs to PEG-PCL diblock polymer *via* acid-detachable *cis*-aconitic anhydride (CAA) bonds. As a negative control, pH-stable Nano-PROTACs (sNano-PROTACs) were synthesized by conjugating PEI-based PROTACs to PEG-PCL *via* acid-stable succinic anhydride bonds, which was confirmed by proton nuclear magnetic resonance (Supporting Information Figs. S5 and S6). Both Nano-PROTACs and sNano-PROTACs nanoparticles were prepared from self-assembly of PEG-PCL-CAA/SA-PEI-based PROTACs copolymer by nanoprecipitation method (Fig. 3A). Dynamic light scattering (DLS) displayed the diameter of Nano-PROTACs around 24.70 ± 2.00 nm and sNano-PROTACs around 25.00 ± 1.61 nm at pH 7.4 (Fig. 3B), which was consistent with transmission electron microscopy (TEM) images (Fig. 3C). The monodispersed spherical Nano-PROTACs nanoparticles were dissociated at pH 6.5 due to the acid-induced bond cleavage, while the morphology of sNano-PROTACs at pH 6.5 was monotonous compared to that at pH 7.4 as shown in Fig. 3C and D. In addition, zeta potentials of Nano-PROTACs and sNano-PROTACs were both negative at pH 7.4 (Fig. 3E). Notably, Nano-PROTACs possessed characteristics of charge reversal from negative potential to positive potential at pH 6.5 due to acid-induced PEI-based PROTACs dissociation, whereas acid medium exhibited negligible influence on zeta potentials of sNano-PROTACs (Fig. 3F). To further demonstrate the acid-responsive feature of Nano-PROTACs, PEI-based PROTACs release from Nano-PROTACs was examined. As shown in Fig. 3G, over 43.6% PEI-based PROTACs was dramatically released from Nano-PROTACs at pH 6.5. In contrast, minimal release was detected in the group of sNano-PROTACs at the acid condition. Besides, both Nano-PROTACs and sNano-PROTACs could maintain their stability in physiological environment for over 7 days (Fig. 3H).

3.3. Nano-PROTACs reprogram glycolysis in vitro

As mentioned in Fig. 2, PEI-based PROTACs could induce HK-2 degradation *via* the UPS pathway, then, we further explored whether pH-activatable Nano-PROTACs also operated the ubiquitination protein degradation or not (Fig. 4A). First, the expression of HK-2 in CT26 cells was evaluated after exposure to Nano-PROTACs for different times to investigate the degradation efficiency. As shown in Fig. 4B−D, the expression of HK-2 in CT26 tumor cells was significantly downregulated with 54.9% after 24 h upon co-incubation with Nano-PROTACs. In contrast, sNano-PROTACs negatively affected HK-2 protein degradation even after 24 h. The poly-ubiquitin of CT26 cells after Nano-PROTACs and sNano-PROTACs treatment was also detected. The Nano-PROTACs group showed higher levels of poly-ubiquitin than the PBS and the sNano-PROTACs group (Supporting Information Fig. S7). Subsequently, considering that the energy metabolism of tumor cells could be reprogrammed after HK-2 protein degradation, a mitochondrial bioenergetic profiles in CT26 cells upon different treatments were investigated using the Seahorse XF96 extracellular flux analyzer. CT26 cells were pretreated with Nano-PROTACs and sNano-PROTACs for 12 h. Then, the extracellular acidification rate (ECAR) was detected in response to sequential incubation with glucose, oligomycin, and 2-deoxy-D-glucose, which could reflect changes in glycolytic activity. Glycolysis was induced by adding saturating quantities of glucose. Subsequently, the maximal glycolysis capacity was obtained by using oligomycin as an ATP synthase inhibitor to eliminate mitochondria oxidative phosphorylation (OXPHOS). Finally, the addition of 2-deoxy-glucose, a competitive inhibitor of HK-2, indicated glycolysis reserve. Fig. 4E−H showed that Nano-PROTACs

CT26 cells (5×10^5) on the flank of BALB/c mice. PBS, PEI-based PROTACs, Nano-PROTACs and sNano-PROTACs were administrated *via* intravenous injection (i.v.) in mice for 6 times interval one day. (B) Relative tumor volume after PEI-based PROTACs, Nano-PROTACs and sNano-PROTACs treatment for five times with an equal dose (LND: 5 mg/kg, THA: 5 mg/kg) in CT26-bearing mice. (C) Relative mice body weights detection and (D) excised tumor weight on Day 14. (E) H&E staining (scale bar = 50 μm) and immunofluorescence staining (Green: TUNEL, caspase 3 and PCNA, Blue: nuclei, scale bar = 50 μm) of CT26 tumors. (F, G) Immunofluorescence staining quantitation of PCNA, active caspase 3. (H) Immunofluorescence staining (Green: HK-2, Blue: nuclei, scale bar = 50 μm) of CT26 tumors. (I) Immunofluorescence staining quantitation of HK-2. (J) Western blot assay and (K) quantitation of HK-2 degradation effect in CT26 tumor lysate. (L) Western blot assay and (M) quantitation of active caspase 3 in CT26 tumor lysate. (N) Western blot assay and (O) quantitation of GSDME-N in CT26 tumor lysate. $^*P < 0.5$, $^{**}P < 0.01$, $^{***}P < 0.001$, $^{****}P < 0.0001$.

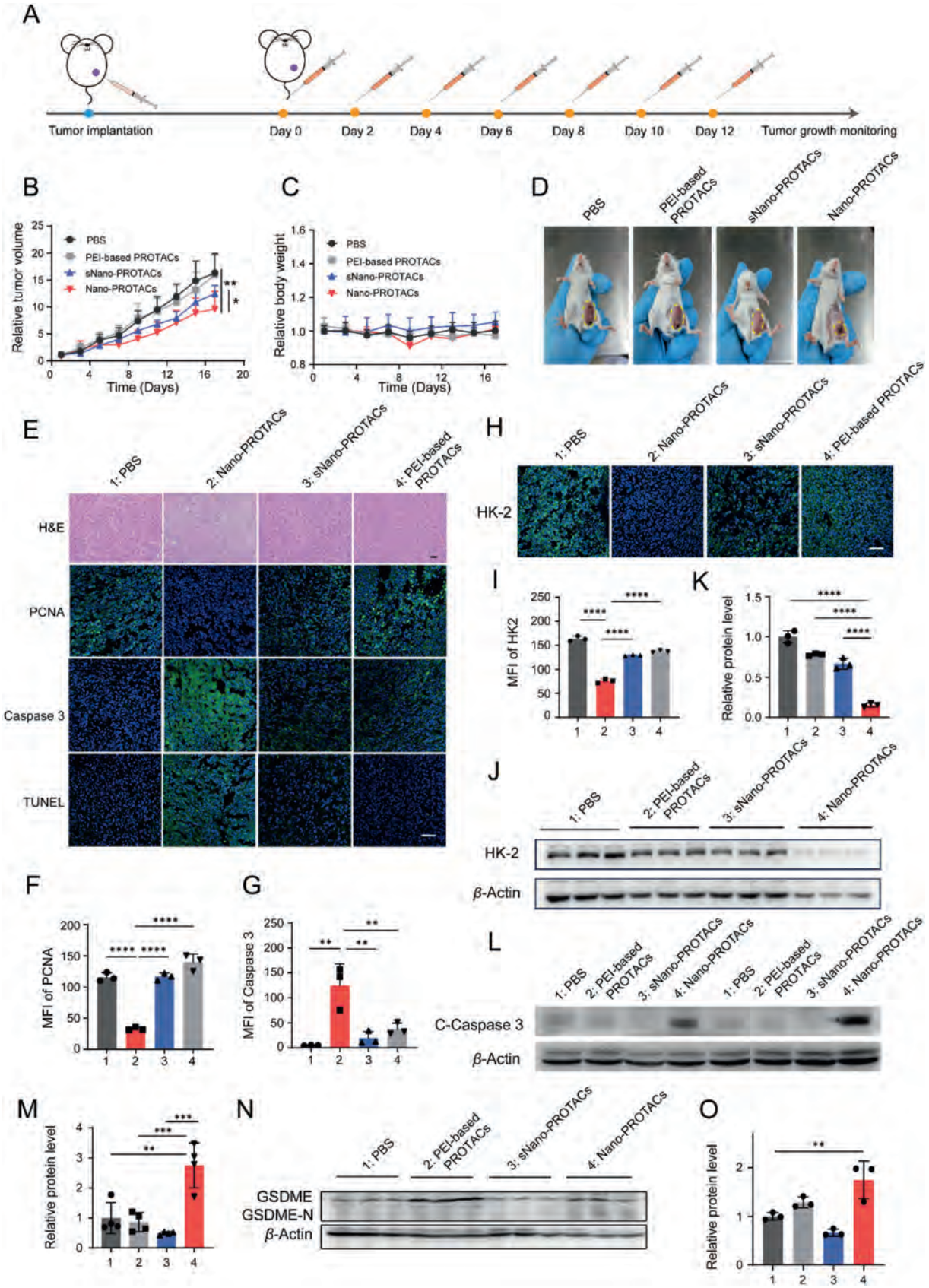

Figure 7 *In vivo* anti-tumor efficacy of Nano-PROTACs in 4T1 orthotopic tumor-bearing mice. (A) Schematic illustration of treatment process. 4T1 orthotopic tumor model was established by injection of 4T1 cells (1×10^6) into the breast pad of the BALB/c mice. PBS, PEI-based PROTACs, sNano-PROTACs and Nano-PROTACs were injected *via* intravenous injection. The growth curves for tumors (B) and body wight

significantly reduced the key index of glycolysis mentioned above compared to PBS and sNano-PROTACs.

Furthermore, we investigated the intracellular behavior and mitochondria targeting capacity of Nano-PROTACs by confocal laser scanning microscope (CLSM). Confocal images showed that Ce6-labeled Nano-PROTACs performed perfect mitochondria colocalization after 3 h incubation with CT26 cells (Fig. 4I). Fluorescence of Nano-PROTACs and mitochondria exhibited almost coincide inside cells (Fig. 4J). Pearson's correlation coefficient value and Mander's colocalization coefficient value of colocalization between mitochondria and Nano-PROTACs were shown in Supporting Information Fig. S8. Then, we detected the permeability of Nano-PROTACs. The results showed that Nano-PROTACs exhibited a better permeability performance than sNano-PROTACs in CT26 tumor spheres under pH 6.5 condition. This higher permeability was specific to pH 6.5 rather than pH 7.4 (Fig. 4K). These results demonstrated that Nano-PROTACs showed the strongest glycolysis inhibition and reprogramming, owing to the perfect mitochondria targeting, improved cellular uptake and HK-2 degradation.

3.4. Nano-PROTACs provoked cytotoxicity via inducing GSDME-dependent pyroptosis

The *in vitro* cytotoxicity of Nano-PROTACs and sNano-PROTACs were investigated on CT26 and 4T1 tumor cells after 24 h by 3-(4,5-dimethylthiazol-2-yl)-2,5-diphenyltetrazolium bromide (MTT) assay. Startling, Nano-PROTACs exhibited a stronger suppression in CT26 and 4T1 tumor cells than sNano-PROTACs (Fig. 5A, Supporting Information Fig. S9 and Table S2), attributed to more PEI-based PROTACs dissociation upon acid-activatable bonds cleavage at endosome/lysosome acid microenvironment, which was consistent with release profiles (Fig. 3G) and WB assay (Fig. 4B) as mentioned above.

Previous studies have shown that LND induced cytotoxicity *via* triggering cell apoptosis[42]. Then, to elucidate if Nano-PROTACs caused cell death *via* the apoptosis pathway, we used an Annexin V-fluorescein 5-isothiocyanate (FITC)/PI staining assay to evaluate the mode of cell death by flow cytometry analysis. As expected, a significant increase in cell apoptosis was found following treatment with Nano-PROTACs. Notably, Nano-PROTACs showed higher early and late apoptosis rates (30.56%) than the control group (8.98%) and sNano-PROTACs (22.52%) in CT26 cells as shown in Fig. 5B and C. A live/dead cell staining assay was adopted to evaluate the cytotoxic effect of Nano-PROTACs on CT26 cells, where the living cells were labeled by calcein-AM (green fluorescence) and dead cells were labeled by PI (red fluorescence). Compared with PBS, free LND and sNano-PROTACs, Nano-PROTACs and PEI-based PROTACs showed a dramatical cytotoxicity, exhibiting that a strong red fluorescent signal was monitored after 24 h (Fig. 5D). Then, we also studied the decrease in mitochondrial membrane potential using JC-1 assay as a fluorescence probe by CLSM, which was another major indicator of apoptosis. Our studies made this clear that mitochondria were destroyed upon treatment with Nano-PROTACs, showing that red fluorescence (the formation of J-aggregates) converted to green fluorescence (the formation of J-monomer). Compared with that of control and sNano-PROTACs, the J-monomers' proportion of Nano-PROTACs increased by 3.8 and 3.4-fold, respectively (Fig. 5E and Supporting Information Fig. S10).

The representative apoptosis-related proteins such as caspase-3 cleavage were detected by WB analysis. Activated caspase-3 was dramatically increased after incubation with Nano-PROTACs, the intensity of which was 2.2-fold that of control (Fig. 5F and G). Amazingly, we observed that the dying cells induced by Nano-PROTACs exhibited significant cell swelling and the formation of large bubbles on the cell membrane (Fig. 5H), which are typical features of pyroptosis[43,44]. In contrast, sNano-PROTACs induced only marginal alternations in cell morphology at the same dose of PEI-based PROTACs. Next, the mechanism of pyroptosis evoked by Nano-PROTACs was investigated. The immunoblots analysis of gasdermin cleavage revealed that Nano-PROTACs triggered increasing GSDME-N fragments in CT26 cells, while negligible GSDME-N fragments were detected after treatment with sNano-PROTACs (Fig. 5I and J). We also detected the cell pyroptosis pathway induced by GSDMD. Supporting Information Fig. S11 shows that Nano-PROTACs couldn't increase GSDMD-N fragments. These results demonstrated that robust pyroptosis and cytotoxicity were induced by Nano-PROTACs through the caspase 3-GSDME pathway. The illustration of the cell death pathway induced by Nano-PROTACs was shown in Fig. 5K.

3.5. Nano-PROTACs achieved robust tumor ablation and minimized toxicity

Given the powerful cytotoxicity and high efficiency pyroptosis of Nano-PROTACs toward tumor cells, we exploited Nano-PROTACs for cancer therapy. The antitumor effect of Nano-PROTACs was investigated using CT26 tumor model. CT26 cells were subcutaneously injected into the back of mice. Nano-PROTACs were intravenously injected at day 0, 2, 4, 6, 8, 10 and 12 after tumor size reached $\sim$50 mm^3 as shown in Fig. 6A. Results showed that Nano-PROTACs produced much better tumor suppression than did sNano-PROTACs and PEI-based PROTACs mediated anti-tumor effect (Fig. 6B). Nano-PROTACs achieved 79.2% tumor eradication, significantly higher values than those saline-treated group (0%) and PEI-based PROTACs (24.9%). These results were further confirmed by *in vivo* tumor photographs and *ex-vivo* weights (Fig. 6D and Supporting Information Fig. S12). The recording of mice body weight revealed no significant difference between Nano-PROTACs and other groups (Fig. 6C). In addition, hematoxylin and eosin staining (H&E) of major organs (heart, liver, spleen, lung, kidney) also showed no dramatical difference after treatment with different groups, in addition to the liver toxicity of PEI-based PROTACs (Supporting Information Fig. S13), indicating that Nano-PROTACs exhibited excellent biosafety.

(C) in mice with the indicated treatments. (D) *In situ* tumor images in mice with the indicated treatments. (E) H&E staining (scale bar = 50 μm) and immunofluorescence staining (Green: TUNEL, caspase 3 and PCNA, Blue: nuclei, scale bar = 50 μm) of 4T1 tumors. (F, G) Immunofluorescence staining quantitation of PCNA, active caspase 3. (H) Immunofluorescence staining (Green: HK-2, Blue: nuclei, scale bar = 50 μm) of 4T1 tumors. (I) Immunofluorescence staining quantitation of HK-2. (J) Western blot assay and (K) quantitation of HK-2 degradation effect in 4T1 tumor lysate. (L) Western blot assay and (M) quantitation of active caspase 3 in 4T1 tumor lysate. (N) Western blot assay and (O) quantitation of GSDME-N in 4T1 tumor lysate. *$P < 0.5$, **$P < 0.01$, ***$P < 0.001$, ****$P < 0.0001$.

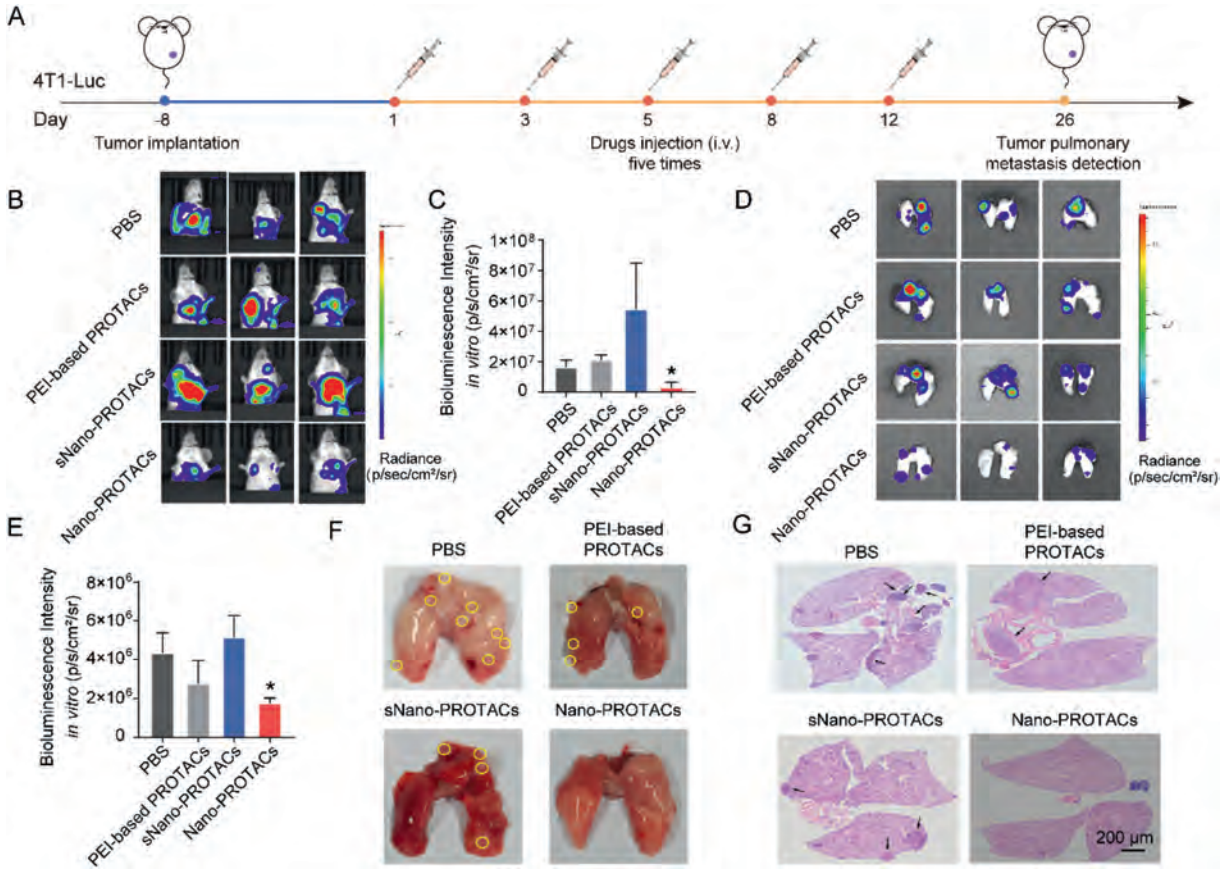

Figure 8 Inhibitory effect of Nano-PROTACs on tumor metastasis. (A) Schematic illustration of treatment process. 4T1 orthotopic tumor-bearing mice were treated with PBS, PEI-based PROTACs, sNano-PROTACs and Nano-PROTACs at the indicated time points. Bioluminescence images (B) and quantitative analysis (C) of metastatic nodules *in vivo* in the lungs from 4T1 orthotopic tumor-bearing mice with the indicated treatments. Bioluminescence images (D) and quantitative analysis (E) of metastatic nodules *ex vivo* in the lungs from 4T1 orthotopic tumor-bearing mice with the indicated treatments. (F) Representative images of isolated lungs in 4T1 orthotopic tumor-bearing mice with the indicated treatments. (G) H&E staining of lung tissues in 4T1 orthotopic tumor-bearing mice with the indicated treatments (scale bar = 200 μm). $^{*}P < 0.5$, $^{**}P < 0.01$, $^{***}P < 0.001$, $^{****}P < 0.0001$.

H&E staining of CT26 tumors exhibited extensive apoptosis and necrosis after treatment with Nano-PROTACs (Fig. 6E). This result was further corroborated by PCNA immunofluorescence staining and TdT-mediated dUTP nick end labeling (TUNEL) assay (Fig. 6E–G). To further explore HK-2 degradation after treatment with Nano-PROTACs *in vivo*, the expression of HK-2 in CT26 tumor cells was examined by immunofluorescence staining and WB analysis. As seen in Fig. 6H–K, Nano-PROTACs provoked a stronger downregulation of HK-2 expression, achieving a 77.9% reduction compared to of the saline group and sNano-PROTACs. sNano-PROTACs did not affect HK-2 expression in CT26 tumors, which was not surprising since PEI-based PROTACs did not dissociate from sNano-PROTACs to perform protein degradation *in vivo*. Expression of caspase 3 and gasdermin E cleavage was also studied *in vivo* as shown in Fig. 6L–O, showing that Nano-PROTACs upregulated the expression of 3.0-fold activated caspase 3 and 1.4-fold GSDME-N fragment compared with that of the saline group.

To further validate the *in vivo* anti-tumor efficacy of pH-activatable engineered nanoparticle-based selective HK-2 degrader, we constructed a 4T1 orthotopic tumor-bearing mouse model by injecting the luciferase-labeled 4T1 cells into the breast pad of BALB/c mice. When tumor size reached 50 mm^3, mice were divided into four groups (PBS, PEI-based PROTACs, sNano-PROTACs and Nano-PROTACs). The treatment schedule was shown in Fig. 7A. Results showed that Nano-PROTACs produced much better tumor suppression than did sNano-PROTACs and PEI-based PROTACs mediated anti-tumor effect (Fig. 7B). Nano-PROTACs achieved 61.2% tumor eradication, significantly higher values than those saline-treated group and PEI-based PROTACs. These results were further confirmed by an *in vivo* tumor photograph (Fig. 7D). The recording of mice body weight revealed no significant difference between Nano-PROTACs and other groups (Fig. 7C), further indicating that Nano-PROTACs exhibited excellent biosafety.

H&E staining of 4T1 tumors exhibited extensive apoptosis and necrosis after treatment with Nano-PROTACs (Fig. 7E). This result was further corroborated by PCNA immunofluorescence staining and TUNEL assay (Fig. 7E–G). To further explore HK-2 degradation after treatment with Nano-PROTACs *in vivo*, the expression of HK-2 in 4T1 tumor cells was examined by immunofluorescence staining and WB analysis. As seen in Fig. 7H–K, Nano-PROTACs provoked stronger downregulation of HK-2 expression, achieving an 84.8% reduction compared to of the

saline group and sNano-PROTACs. Expression of caspase 3 and gasdermin E cleavage were also studied *in vivo* as shown in Fig. 7L−O, showing that Nano-PROTACs upregulated the expression of 2.8-fold activated caspase 3 and 1.7-fold GSDME-N fragment compared with that of saline group. Collectively, these results demonstrated the potent antitumor ability of Nano-PROTACs *via* inducing tumor cell pyroptosis and reprogramming glycolysis, with no obvious adverse effects. However, in-depth mechanisms of pyroptosis induced by Nano-PROTACs should be explored in the future.

3.6. Nano-PROTACs inhibited pulmonary metastasis

Inhibiting glycolysis is critical for reprogramming the tumor microenvironment, which intimates closely with tumor metastasis. Thus, we evaluated the effect of Nano-PROTACs on *in vivo* anti-tumor metastasis ability by monitoring pulmonary metastasis using a 4T1 orthotopic tumor-bearing mouse model. When tumor volume reached 50 mm^3, PEI-based PROTACs, sNano-PROTACs and Nano-PROTACs were injected *via* intravenous injection into mice once every two days for five times. The treatment schedule was shown in Fig. 8A. Next, we observed the pulmonary metastasis *in vivo* and *ex vivo* by bioluminescence imaging. As shown in Fig. 8B−E, the bioluminescence intensity of lungs in the Nano-PROTACs-treated mice was lower than in PBS- and PEI-based PROTACs-treated mice, indicating that Nano-PROTACs exhibited a potent inhibitory effect on pulmonary metastasis. Meanwhile, we also found that Nano-PROTACs-treated mice had fewer tumor nodules on the surface of their lungs than PBS- or PEI-based PROTACs-treated mice (Fig. 8F and G). These results further supported that Nano-PROTACs had potent capacity for tumor growth and pulmonary metastasis inhibition.

4. Conclusions

In summary, we successfully constructed a novel pH-activatable engineered nanoparticle-based selective protein degrader platform that harnessed UPS with pH-activated protein degradation for cancer therapy. Nano-PROTACs specifically blocked the glycolysis metabolism *via* targeted proteolysis of HK-2, representing a distinct type of glucose metabolism therapy nano-agents. Our platform afforded the following advantages, including flexible ligand ratio regulation, pH-activatable protein degradation ability, increased tumor accumulation, deep tumor penetration and increased protein degradation extent. Importantly, Nano-PROTACs could specifically evoke GSDME-mediated pyroptosis to enhance cancer therapy. Consequently, Nano-PROTACs exhibited superior CT26 and 4T1 tumor shrinkage and pulmonary metastasis inhibition without obvious systemic toxicity. Taken together, the proposed Nano-PROTACs platform might afford a novel therapeutic modality to potentiate cancer therapy.

Acknowledgements

This research was financially supported by the Shenzhen Science and Technology Program (JCYJ20230807145605011, China), the National Natural Science Foundation of China (NSFC) grants (82003691), Natural Science Basic Research Program of Shaanxi (2025JC-YBQN-1051, China), the Innovation Capability Support Program of Shaanxi (2023-CX-TD-72, China) and Key Research and Development Project of Shaanxi Province (2023-YBSF-121, China). We thank Prof. Yiguang Wang (School of Pharmaceutical Sciences, Peking University, Beijing, China) for kindly providing the murine luciferase-expressing 4T1 cells.

Author contributions

Dechun Liu designed the research. Linlin Gong, Shasha Li, Jiahui Sun, Kunhong Liu and Simeng Wang performed the experiments and analyzed the data. Li Yan, Meiju Ji, Peng Hou, Dan Yang, and Dechun Liu discussed the data. Linlin Gong and Shasha Li wrote the paper. Dechun Liu conceived the project. Dechun Liu revised the paper. All of the authors have read and approved the final manuscript.

Conflicts of interest

The authors have no conflicts of interest to declare.

Appendix A. Supporting information

Supporting information to this article can be found online at https://doi.org/10.1016/j.apsb.2025.11.002.

References

1. Vander Heiden MG, Cantley LC, Thompson CB. Understanding the Warburg effect: the metabolic requirements of cell proliferation. *Science (New York, NY)* 2009;**324**:1029−33.
2. Guo D, Tong Y, Jiang X, Meng Y, Jiang H, Du L, et al. Aerobic glycolysis promotes tumor immune evasion by hexokinase2-mediated phosphorylation of I$\kappa B\alpha$. *Cell Metab* 2022;**34**:1312-24.e6.
3. Guo X, Li H, Xu H, Woo S, Dong H, Lu F, et al. Glycolysis in the control of blood glucose homeostasis. *Acta Pharm Sin B* 2012;**2**: 358−67.
4. Hanahan D. Hallmarks of cancer: new dimensions. *Cancer Discov* 2022;**12**:31−46.
5. Patra KC, Wang Q, Bhaskar PT, Miller L, Wang Z, Wheaton W, et al. Hexokinase 2 is required for tumor initiation and maintenance and its systemic deletion is therapeutic in mouse models of cancer. *Cancer Cell* 2013;**24**:213−28.
6. Xu S, Catapang A, Doh HM, Bayley NA, Lee JT, Braas D, et al. Hexokinase 2 is targetable for HK1 negative, HK2 positive tumors from a wide variety of tissues of origin. *J Nucl Med* 2018;**60**:212−7.
7. Fang J, Luo S, Lu Z. HK2: gatekeeping microglial activity by tuning glucose metabolism and mitochondrial functions. *Mol cell* 2023;**83**: 829−31.
8. Bononi G, Masoni S, Di Bussolo V, Tuccinardi T, Granchi C, Minutolo F. Historical perspective of tumor glycolysis: a century with Otto Warburg. *Semin Cancer Biol* 2022;**86**:325−33.
9. Shoshan-Barmatz V, Golan M. Mitochondrial VDAC1: function in cell life and death and a target for cancer therapy. *Curr Med Chem* 2012; **19**:714−35.
10. Arif T, Vasilkovsky L, Refaely Y, Konson A, Shoshan-Barmatz V. Silencing VDAC1 expression by siRNA inhibits cancer cell proliferation and tumor growth in vivo. *Mol Ther Nucleic Acids* 2014;**3**:e159.
11. Singh D, Banerji AK, Dwarakanath BS, Tripathi RP, Gupta JP, Mathew TL, et al. Optimizing cancer radiotherapy with 2-deoxy-D-glucose dose escalation studies in patients with glioblastoma multiforme. *Strahlenther Onkol* 2005;**181**:507−14.
12. Jiao L, Zhang HL, Li DD, Yang KL, Tang J, Li X, et al. Regulation of glycolytic metabolism by autophagy in liver cancer involves selective autophagic degradation of HK2 (hexokinase 2). *Autophagy* 2018;**14**: 671−84.
13. Wang F, Ogasawara MA, Huang P. Small mitochondria-targeting molecules as anti-cancer agents. *Mol Aspect Med* 2010;**31**:75−92.

14. Cheng G, Zhang Q, Pan J, Lee Y, Ouari O, Hardy M, et al. Targeting lonidamine to mitochondria mitigates lung tumorigenesis and brain metastasis. *Nat Commun* 2019;**10**:2205.
15. Mansi JL, de Graeff A, Newell DR, Glaholm J, Button D, Leach MO, et al. A phase II clinical and pharmacokinetic study of Lonidamine in patients with advanced breast cancer. *Br J Cancer* 1991;**64**:593−7.
16. Lai AC, Crews CM. Induced protein degradation: an emerging drug discovery paradigm. *Nat Rev Drug Discov* 2017;**16**:101−14.
17. Dale B, Cheng M, Park KS, Kaniskan H, Xiong Y, Jin J. Advancing targeted protein degradation for cancer therapy. *Nat Rev Cancer* 2021; **21**:638−54.
18. Chamberlain PP, Hamann LG. Development of targeted protein degradation therapeutics. *Nat Chem Biol* 2019;**15**:937−44.
19. Burslem GM, Crews CM. Proteolysis-targeting chimeras as therapeutics and tools for biological discovery. *Cell* 2020;**181**:102−14.
20. Backus KM, Correia BE, Lum KM, Forli S, Horning BD, González-Páez GE, et al. Proteome-wide covalent ligand discovery in native biological systems. *Nature* 2016;**534**:570−4.
21. Popovic D, Vucic D, Dikic I. Ubiquitination in disease pathogenesis and treatment. *Nat Med* 2014;**20**:1242−53.
22. Farnaby W, Koegl M, Roy MJ, Whitworth C, Diers E, Trainor N, et al. BAF complex vulnerabilities in cancer demonstrated *via* structure-based PROTAC design. *Nat Chem Biol* 2019;**15**:672−80.
23. Gadd MS, Testa A, Lucas X, Chan KH, Chen W, Lamont DJ, et al. Structural basis of PROTAC cooperative recognition for selective protein degradation. *Nat Chem Biol* 2017;**13**:514−21.
24. Schapira M, Calabrese MF, Bullock AN, Crews CM. Targeted protein degradation: expanding the toolbox. *Nat Rev Drug Discov* 2019;**18**: 949−63.
25. Neklesa TK, Winkler JD, Crews CM. Targeted protein degradation by PROTACs. *Pharmacol Ther* 2017;**174**:138−44.
26. Bushweller JH. Targeting transcription factors in cancer—from undruggable to reality. *Nat Rev Cancer* 2019;**19**:611−24.
27. Moreau K, Coen M, Zhang AX, Pachl F, Castaldi MP, Dahl G, et al. Proteolysis-targeting chimeras in drug development: a safety perspective. *Br J Pharmacol* 2020;**177**:1709−18.
28. Reynders M, Trauner D. PHOTACs enable optical control of protein degradation. *Methods Mol Biol* 2021;**2365**:315−29.
29. Li JC, Yu XR, Shi XY, Shen MW. Cancer nanomedicine based on polyethylenimine-mediated multifunctional nanosystems. *Prog Mater Sci* 2022;**124**:100871.
30. Yang S, Wu Y, Zhong W, Chen R, Wang M, Chen M. GSH/Ph dual activatable crosslinked and fluorinated pei for cancer gene therapy through endogenous iron de-hijacking and *in situ* ROS amplification. *Adv Mater* 2023;**36**:e2304098.
31. Liu D, Fu L, Gong L, Li S, Li K, Liu K, et al. Proton-gradient-driven porphyrin-based liposome remote-loaded with imiquimod as *in situ* nanoadjuvants for synergistically augmented tumor photo-immunotherapy. *ACS Appl Mater* 2024;**16**:8403−16.
32. Liu D, Li K, Gong L, Fu L, Yang D. Charge reversal yolk-shell liposome co-loaded JQ1 and doxorubicin with high drug loading and optimal ratio for synergistically enhanced tumor chemo-immunotherapy *via* blockade PD-L1 pathway. *Int J Pharm* 2023; **635**:122728.
33. Liu DC, Chen BL, Mo YL, Wang ZH, Qi T, Zhang Q, et al. Redox-activated porphyrin-based liposome remote-loaded with indoleamine 2,3-dioxygenase (IDO) inhibitor for synergistic photoimmunotherapy through induction of immunogenic cell death and blockage of IDO pathway. *Nano Lett* 2019;**19**:6964−76.
34. Yang D, Feng Y, Yuan Y, Zhang L, Zhou Y, Midgley AC, et al. Protein coronas derived from mucus Act as both spear and shield to regulate transferrin functionalized nanoparticle transcellular transport in enterocytes. *ACS Nano* 2024;**18**:7455−72.
35. Li HJ, Du JZ, Liu J, Du XJ, Shen S, Zhu YH, et al. Smart superstructures with ultrahigh pH-sensitivity for targeting acidic tumor microenvironment: instantaneous size switching and improved tumor penetration. *ACS Nano* 2016;**10**:6753−61.
36. Li HJ, Du JZ, Du XJ, Xu CF, Sun CY, Wang HX, et al. Stimuli-responsive clustered nanoparticles for improved tumor penetration and therapeutic efficacy. *Proc Natl Acad Sci USA* 2016;**113**:4164−9.
37. Zhang C, Zeng Z, Cui D, He S, Jiang Y, Li J, et al. Semiconducting polymer Nano-PROTACs for activatable photo-immunometabolic cancer therapy. *Nat Commun* 2021;**12**:2934.
38. Gao J, Hou B, Zhu Q, Yang L, Jiang X, Zou Z, et al. Engineered bioorthogonal POLY-PROTAC nanoparticles for tumour-specific protein degradation and precise cancer therapy. *Nat Commun* 2022;**13**: 4318.
39. Cao Z, Liu J, Yang X. Deformable nanocarriers for enhanced drug delivery and cancer therapy. *Explorations* 2024;**4**:20230037.
40. Liu J, Zhou Y, Lyu Q, Yao X, Wang W. Targeted protein delivery based on stimuli-triggered nanomedicine. *Explorations* 2024;**4**: 20230025.
41. De Lena M, Lorusso V, Latorre A, Fanizza G, Gargano G, Caporusso L, et al. Paclitaxel, cisplatin and lonidamine in advanced ovarian cancer. A phase II study. *Eur J Cancer* 2001;**37**:364−8.
42. Ravagnan L, Marzo I, Costantini P, Susin SA, Zamzami N, Petit PX, et al. Lonidamine triggers apoptosis *via* a direct, Bcl-2-inhibited effect on the mitochondrial permeability transition pore. *Oncogene* 1999;**18**: 2537−46.
43. Bergsbaken T, Fink SL, Cookson BT. Pyroptosis: host cell death and inflammation. *Nat Rev Microbiol* 2009;**7**:99−109.
44. Shi J, Zhao Y, Wang K, Shi X, Wang Y, Huang H, et al. Cleavage of GSDMD by inflammatory caspases determines pyroptotic cell death. *Nature* 2015;**526**:660−5.